Received December 8, 2018, accepted December 20, 2018, date of publication December 27, 2018,
date of current version January 23, 2019.

Digital Object Identifier 10.1109/ACCESS.2018.2889997

Vehicle Stability Control Based on Model Predictive Control Considering the Changing Trend of Tire Force Over the Prediction Horizon

SHAOSONG LI, GUODONG WANG, BANGCHENG ZHANG, ZHIXIN YU, AND GAOJIAN CUI
School of Mechatronic Engineering, Changchun University of Technology, Changchun 130012, China

Corresponding author: Bangcheng Zhang (zhangbangcheng@ccut.edu.cn)

This work was supported in part by the National Natural Science Foundation of China under Grant 61603060 and Grant 61751304, in part by the Jilin Province Science and Technology Fund for Young Scholars under Grant 20170520097JH and Grant 20160520106JH, in part by the Key Technology on Major Program of Jilin Province under Grant 20170201005GX, in part by the Science and Technology Research Planning Project of the Education Department of Jilin Province under Grant JJKH20181035KJ, and in part by the Science and Technology Bureau Project of Changchun under Grant 16CX21.

ABSTRACT This paper proposes a vehicle stability control approach based on time-varying model predictive control to enhance the handling and stability of active front steering vehicle at the vehicle dynamics limits. The prediction equation of the proposed controller is designed based on the changing trend of tire force over the prediction horizon. Therefore, the prediction equation can represent the nonlinear characteristics in the process of prediction. To verify the effectiveness of the proposed control strategy, nonlinear model predictive controller, and previous linear time-varying model predictive controller are designed and used for comparison. Simulation experiments are performed based on the cosimulation environment of MATLAB and CarSim. At the handling limits, the control performance of the proposed controller exhibited significant improvement compared with the previous one. Moreover, its performance was close to that of the nonlinear controller, whereas its calculation speed is much faster than that of the nonlinear model predictive controller.

INDEX TERMS Active front steering, handling stability, model predictive control, vehicle dynamics.

I. INTRODUCTION

The application of active safety systems in modern vehicles can effectively improve vehicle handling, stability, and comfort performance [1]. Moreover, many production vehicles have used various advanced active chassis control systems, such as anti-lock braking system, electronic stability control, and active front steering (AFS) system. Vehicle dynamics control systems can be classified into three areas, such as longitudinal, lateral, and yaw control. This work focuses on vehicle handling and yaw stability control. AFS developed by BMW in 2003 [2] is an effective way to improve the yaw stability of the vehicle. The main feature of AFS is to generate yaw moment by steering instead of braking. AFS can modify the steering angle of the vehicle without the driver's intervention and does not affect the longitudinal dynamics of vehicle [2]–[6]. With the emergence of intelligent control systems such as lane centering control, more and more production vehicles are equipped with AFS. This provides an opportunity to utilize AFS in stability control [7].

A large number of studies have been carried out on AFS-based vehicle stability control [8]–[12]. Control methods, such as sliding mode control, fuzzy control, and model predictive control, have been applied to the AFS control. Model predictive control (MPC) exploits a system dynamics model to predict the future system evolution and select the best control action with respect to a specified performance criterion [13], [14]. MPC offers a method to deal with constrained optimization problems [15]. Therefore, the accuracy of the established model directly affects the control performance of MPC.

For vehicle dynamics, tire forces provide the primary external influence and can directly influence the handling and stability of a vehicle [16]. The highly nonlinear behavior of tire forces will cause the largest variation in vehicle handling properties throughout the longitudinal and lateral maneuvering range [12]. When vehicle drives with a small lateral acceleration, tire forces are in the linear region. Thus, a linear tire model can be used for MPC to design the AFS controller, which can reduce the computational burden of MPC.

However, when the vehicle steers at a high speed, the lateral acceleration is high, and the tire force begins to saturate and enter the nonlinear region. Linear tire models no longer reflect real change trend of tire forces. Therefore, using a realistic nonlinear tire model is important [16], [17]. However, nonlinear MPC (NMPC) requires the on-line solution of a nonconvex, constrained nonlinear optimization problem, and the calculation burden is large [18], [19].

Linear time-varying MPC (LTVMPC) method [19]–[21] is a widely used method which can take into account the nonlinearity and real-time performance of the system. Choi and Choi [22] proposed a layered vehicle lateral stability control method based on MPC. The lower layer controller distributes the steering angle and braking force according to the corrective yaw moment calculated by upper controller. They linearized the tire model continuously at the operating point and the yaw rate is constrainted to avoid the saturation of the force in tires. The MPC optimization problem is solved by matrix inversion. The results of CarSim simulation shown that the control strategy can track the reference yaw rate in both high and low tire-road friction coefficient. Similar tire force linearization methods can be found in [15] and [23]. Jalali *et al.* [7] developed a steering and braking integrated vehicle stability control method based on MPC. They used a linear tire model and estimated the tire cornering stiffness on the basis of real-time measurements of vehicle's lateral and yaw accelerations. The vehicle stability and the controller feasibility are guaranteed by the soft constraints of system states. The performance of the designed controller was demonstrated by software simulation and Chevrolet experiment testing. However, these linearized tire model is constant over the prediction horizon, which cannot describe the nonlinear characteristics of tire force. We named this approach as simple LTVMPC (S-LTVMPC).

In fact, S-LTVMPC is an effective method for vehicle stability control and there are many research achievements. It mainly restrains tire slip angle or yaw rate to ensure vehicle stability at the handing limits. However, the mandatory stability constraint will make the tire force not be fully utilized. Erlien textitet al. [24] and Funke *et al.* [25] proposed that enforcing the stabilization criteria does not necessarily assist collision avoidance and may conflict with the demands of the desired trajectory, and the controller should allow vehicles to operate outside safety constraints to avoid collision with obstacles. Brown *et al.* [26] proposed a control strategy that integrates local path planning and path tracking using MPC. They linearized the rear tire force in the prediction horizon based on the sequence of tire slip angle from the last step and they allow the vehicle to operate outside of the safety constraint temporarily when the vehicle is in collision avoidance. However, using only the tire slip angle from the previous step will lead to jitter. Funke *et al.* [25] developed a form of regularization of predicted tire slip angles based on an average of the previous predicted tire slip angle and resulting solution to solve this problem. Experiments have shown that the controller is effective both at the handing limits and avoiding sudden obstacles.

In this work, a novel LTVMPC approach considering the changing trend of tire force in the prediction horizon is proposed to extend the feasible range of AFS vehicle, in which the tire model is continuously updated over the prediction horizon according to the nonlinear tendency of tire force. This method does not impose mandatory stability constraints and can fully utilize the tire force, which can avoid the vehicle out of control at the handing limits and can achieve the control effect of NMPC. In addition, the time-varying reference considering the nonlinear tracking target is introduced on the prediction horizon on the basis of our previous work [27]. To verify the control performance of the proposed MPC, we also designed S-LTVMPC and NMPC to compare with the method used in this paper.

This paper is organized as follows. Section II introduces the overall control architecture of the proposed controllers. Section III builds the vehicle and tire model and contains details associated with control problems. Section IV designs the model predictive controllers. Section V reveals the simulation results and compares the control effects of S-LTVMPC, NMPC and the proposed LTVMPC method under different conditions. The conclusion and future work are summarized in Section VI.

II. OVERALL CONTROL ARCHITECTURE

This section describes the overall control structure and internal submodules of the proposed controller. Fig. 1 shows the structure of the proposed controllers, which consists of a reference model, an MPC controller and a simulation vehicle model. The reference model is designed to calculate the reference yaw rate according to driver's steering input δ_{fdri}, which will be discussed in detail in Section III-C. MPC controller optimizes the front steering angle according to the reference yaw rate and current vehicle status parameters. CarSim vehicle model is the controlled object. Its input is the front steering angle δ_f, and the outputs are yaw rate γ, vehicle sideslip angle β, and longitudinal velocity V_x.

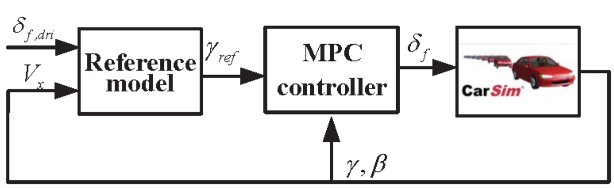

FIGURE 1. Flow structure of the control system.

III. SYSTEM MODELING AND CONTROL PROBLEM STATEMENT

A. VEHICLE MODEL

The prediction model used in this paper is a simplified bicycle model, as shown in Fig. 2. The frame origin is at the vehicle center of mass, with x-axis along the vehicle longitudinal direction pointing forward, y-axis pointing to the left vehicle

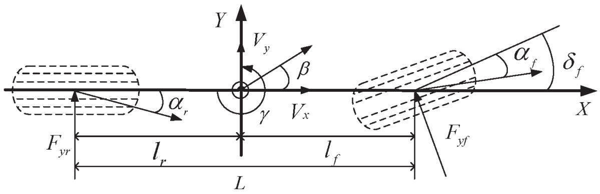

FIGURE 2. Vehicle dynamic model.

side, and z-axis pointing upward [3]. l_f and l_r are the distances from vehicle mass center to the front and rear axles, respectively; $F_{y,f}$ and $F_{y,r}$ refer to the lateral force at the front and rear tires, respectively; β denotes the vehicle sideslip angle; γ indicates the vehicle yaw rate; V_x and V_y are the longitudinal and lateral velocity of the vehicle, respectively; δ_f denotes the front steering angle; and α_f and α_r refer to the slip angle of the front and rear tires, respectively. To describe the vehicle dynamics, we make the following assumptions [28], [29]:

- Ignore the influence of the steering system and directly take the front steering angle δ_f as the input.
- Ignore the effect of suspension, that is, the displacement along the z-axis, the pitch angle around the y-axis, and the roll angle around the x-axis are zero.
- Ignore the influence of the longitudinal force and load change.
- Ignore aerodynamic effects.

From the above-mentioned hypothesis, the equations of lateral and yaw motion of vehicle are described as follow:

$$\begin{aligned} m(\dot{V}_y + V_x\gamma) &= F_{y,f} + F_{y,r} \\ I_z\dot{\gamma} &= l_f F_{y,f} - l_r F_{y,r} \end{aligned} \tag{1}$$

where m is the vehicle mass, and I_z represents the yaw moment of inertia.

Due to the influence of tire longitudinal force is ignored in this study, the lateral tire force is calculated by the tire model with pure lateral slip condition:

$$F_{y,j} = f_{y,j}(\alpha_j, \mu, F_{z,j}) \tag{2}$$

where $f_{y,j}(\cdot)$ is a complex nonlinear function described in the next section, subscript $j = f, r$, refers to the front or rear tire, and μ is the tire-road friction coefficient. Many studies have been conducted on the estimation of tire-road friction coefficient. In this paper, we do not estimate the tire-road friction coefficient and consider it as a known variable.

The tire slip angle are defined as follows:

$$\begin{aligned} \alpha_f &= \arctan\left(\frac{V_y + \gamma l_f}{V_x}\right) - \delta_f \\ &= \beta + \frac{\gamma l_f}{V_x} - \delta_f \\ \alpha_r &= \arctan\left(\frac{V_y - \gamma l_r}{V_x}\right) \\ &= \beta - \frac{\gamma l_r}{V_x} \end{aligned} \tag{3}$$

Considering that the longitudinal velocity of the vehicle is constant and the lateral force at front and rear tires in the bicycle model refers to the lateral forces at the front and rear axles in 4-wheel vehicle. The effects of the pitch rate and roll rate on the distribution of the normal tire load are ignored, the expressions are as follows:

$$\begin{aligned} F_{z,f} &= \frac{mgl_r}{l_f + l_r} \\ F_{z,r} &= \frac{mgl_f}{l_f + l_r} \end{aligned} \tag{4}$$

B. TIRE MODEL

The tire model used in this paper is Pacejka model [30], which is a complex, semi-empirical model. The lateral force depend on normal tire load, tire slip angle and tire-road friction coefficient. The curves of normalized lateral tire forces $F_y/F_{z,N}$ in different tire-road friction coefficients and normal tire loads are shown in Fig. 3. Here, μ is the tire-road friction coefficient; F_z refers to the normal tire load; $F_{z,N}$ indicates the nominal normal tire load, and $F_{z,N} = 6000$ N.

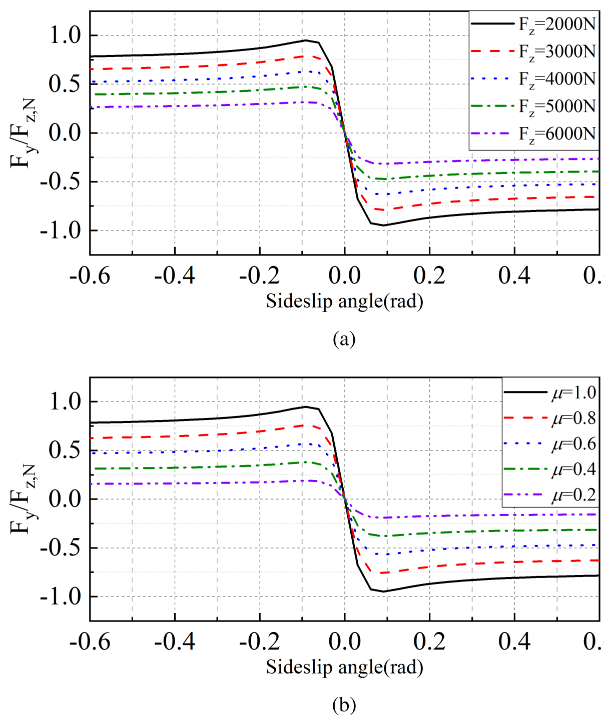

FIGURE 3. Lateral tire force characteristics. (a) Normalized lateral tire forces in different normal tire load. (b) Normalized lateral tire forces in different road friction coefficients.

The lateral tire force can be calculated as follows:

$$\begin{aligned} F_{y,j} &= \mu D \sin(C atan(B\alpha_j - E(B\alpha_j - \alpha_j atan(B\alpha_j)))) \\ B &= \frac{a_3 \sin\left(2atan\left(F_{z,j}/a_4\right)\right)}{CD} \\ C &= a_0 \\ D &= a_1 {F_{z,j}}^2 + a_2 F_{z,j} \\ E &= a_5 F_{z,j} + a_6 \end{aligned} \tag{5}$$

where subscript $j = f, r$, refers to the front or rear tires; $a_0 = 1.75$, $a_1 = 0$, $a_2 = 1000$, $a_3 = 1289$, $a_4 = 7.11$, $a_5 = 0.0053$, and $a_6 = 0.1952$, these constants were obtained by calibration with CarSim based on literature [30], [31].

C. CONTROL PROBLEM STATEMENTS

1) Constraints of the controller: In the control process, system constraints, such as the physical limits of the actuators, should be considered. The constraint of front steering angle is expressed by the following inequality:

$$-\delta_{f\,\max} \le \delta_f(k) \le \delta_{f\,\max} \tag{6}$$

Moreover, the change rate of the front steering angle is constrained to obtain a smooth control command sequence as follows:

$$-\Delta\delta_{f\,\max} \le \Delta\delta_f(k) \le \Delta\delta_{f\,\max} \tag{7}$$

2) Reference model: In terms of vehicle dynamics, yaw rate is closely related to the handling stability of vehicle. Hence, yaw rate is used as the control target in this paper, and the reference model is designed based on road condition with a tire-road friction coefficient of 0.85 to determine the reference yaw rate.

The transfer function is derived from the front steering angle that generated by the driver to the yaw rate as follows [32]:

$$\frac{\gamma_{ref\,(s)}}{\delta_{f,dri\,(s)}} = \frac{w_n^2 G_\omega(s)}{s^2 + 2w_n\xi s + w_n^2} \tag{8}$$

where γ_{ref} is the reference yaw rate, $\delta_{f,dri}$ is the driver's output, w_n represents the natural frequency of the vehicle system, ξ indicates the damping coefficient, $G_\omega(s)$ denotes the steady gain transfer functions of γ_{ref} and $\delta_{f,dri}$, and K_ω is the stability factor. These values are calculated as follows:

$$\xi = \frac{m\left(l_f{}^2 C_f + l_r{}^2 C_r\right) + I_z\left(C_f + C_r\right)}{2\left(l_f + l_r\right)\sqrt{mI_z C_f C_r\left(1 + K_\omega V_x^2\right)}}$$

$$w_n = \frac{2\left(l_f + l_r\right)}{V_x}\sqrt{\frac{C_f C_r\left(1 + K_\omega V_x^2\right)}{mI_z}}$$

$$G_\omega(s) = \frac{mV_x^2 l_f}{2C_r\left(l_f + l_r\right)^2\left(1 + K_\omega V_x^2\right)} s + \frac{V_x}{\left(l_f + l_r\right)\left(1 + K_\omega V_x^2\right)}$$

$$K_\omega = -\frac{m\left(l_f C_f - l_r C_r\right)}{2C_f C_r\left(l_f + l_r\right)^2}$$

where C_f and C_r are the cornering stiffness of the front and rear tires, respectively.

Finally, the reference model can be defined as follows:

$$\gamma_{ref\,(s)} = \frac{w_d^2 G_{k\omega}(s)}{s^2 + 2w_d\xi_d s + w_d^2} \cdot \delta_{f,dri\,(s)} \tag{9}$$

where $w_d = k_1 w_n$, $\xi_d = k_2\xi$, $G_{k\omega}(s) = k_3 G_\omega(s)$. k_1, k_2 and k_3 are adjustable parameters that improve the phase delay and response speed of the system. Their values are follows: $k_1 = 1.9$, $k_2 = 1.3$ and $k_3 = 0.8$.

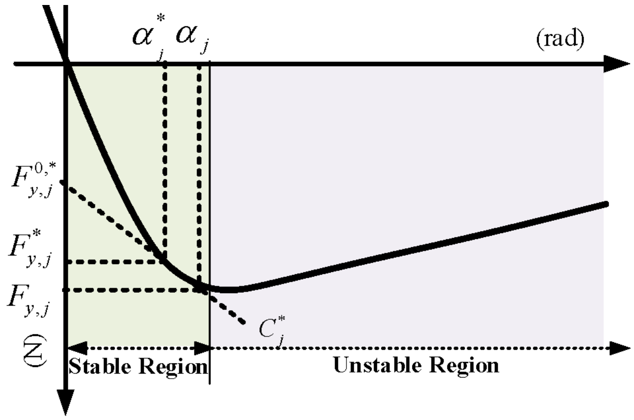

FIGURE 4. Linearization of tire force.

The control problem in this paper is summarized to track the desired yaw rate γ_{ref} in (9), avoid control action saturation and maintain smooth steering by satisfying the constraints in (6) and (7).

IV. MODEL PREDICTIVE CONTROLLER DESIGN

A. S-LTVMPC CONTROLLER DESIGN

The prediction model for S-LTVMPC is built based on the linearized tire model introduced in a previous study [22]. The lateral force of the front and rear tires on the basis of Pacejka tire model are successive linearization at every sample time as follows:

$$F_{y,j} = F_{y,j}^{0,*} + C_j^*\alpha_j \tag{10}$$

where $j = f, r$, refers to the front or rear tires; C_j^* denotes the gradients of the lateral force at the current tire slip angle α_j^*; and $F_{y,j}^{0,*}$ indicates the residual lateral forces (Fig. 4). $F_{y,j}^{0,*}$ is calculated as follows:

$$F_{y,j}^{0,*} = F_{y,j}^* - C_j^*\alpha_j^* \tag{11}$$

where $F_{y,j}^*$ denotes the lateral tire force at the current tire slip angle α_j^*, and $F_{y,j}^*$, C_j^* values are provided by look-up tables.

In addition, the stable and unstable regions in the tire force in Fig. 4 will be discussed later.

In this paper, look-up tables are designed to provide lateral tire forces and the gradients of lateral force for the linear time-varying systems. Fig. 5 shows the 3D map of the lateral tire force under different tire-road friction coefficients. Fig. 6 shows the 3D map of the lateral tire force gradient under different tire-road friction coefficients.

On the basis of the linearized tire model, the prediction model for LTV-MPC is written as follows:

$$\dot{\gamma} = \frac{l_f{}^2 C_f^* + l_r{}^2 C_r^*}{V_x I_z} \cdot \gamma + \frac{l_f C_f^* - l_r C_r^*}{I_z} \cdot \beta - \frac{l_f C_f^*}{I_z} \cdot \delta_f + \frac{l_f}{I_z} \cdot F_{y,f}^{0,*} - \frac{l_r}{I_z} \cdot F_{y,r}^{0,*} \tag{12}$$

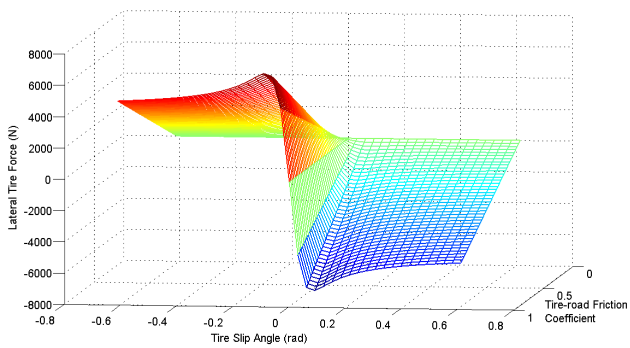

FIGURE 5. 3D map of lateral tire force.

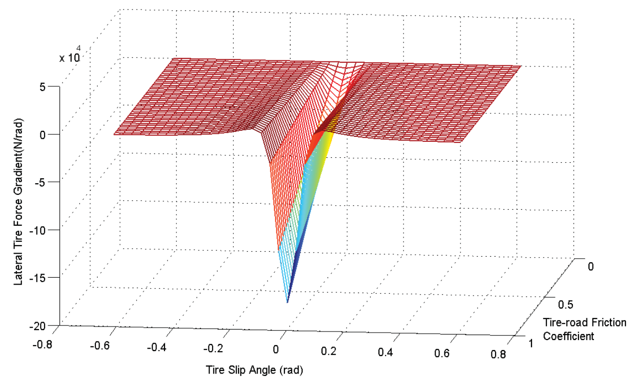

FIGURE 6. 3D map of lateral tire force gradient.

The prediction model can be written in state-space form, as follows:

$$\begin{aligned} \dot{x}(t) &= \mathbf{A}x(t) + \mathbf{B_u}u(t) + \mathbf{B_d}d(t) \\ y(t) &= \mathbf{C}x(t) \end{aligned} \tag{13}$$

where the state variable x is the yaw rate γ, control input u is the front steering angle δ_f, the output vector $y = \gamma$, and disturbance inputs d are the vehicle sideslip angle β and residual lateral forces $F_{y,f}^{0,*}$ and $F_{y,r}^{0,*}$. Output matrix $\mathbf{C} = 1$; State matrix $\mathbf{A}$, input matrix $\mathbf{B_u}$, and disturbance input matrix $\mathbf{B_d}$ are shown as follows:

$$\begin{aligned} \mathbf{A} &= \left[\frac{{l_f}^2 C_f^* + {l_r}^2 C_r^*}{V_x I_z} \right] \\ \mathbf{B_u} &= \left[-\frac{l_f C_f^*}{I_z} \right] \\ \mathbf{B_d} &= \left[\frac{l_f C_f^* - l_r C_r^*}{I_z}, \frac{l_f}{I_z}, -\frac{l_r}{I_z} \right] \end{aligned}$$

For S-LTVMPC, $\mathbf{A}$, $\mathbf{B_u}$, and $\mathbf{B_d}$ remain constant over the prediction horizon.

Discrete (13) with time step T_s and the incremental discrete time model is given as follows:

$$\begin{aligned} \Delta x(k+1) &= \mathbf{A_c}\Delta x(k) + \mathbf{B_{cu}}\Delta u(k) + \mathbf{B_{cd}}\Delta d(k) \\ y(k) &= \mathbf{C}\Delta x(k) + y(k-1) \end{aligned} \tag{14}$$

where

$$\begin{aligned} \Delta x(k) &= x(k) - x(k-1) \\ \Delta u(k) &= u(k) - u(k-1) \\ \Delta d(k) &= d(k) - d(k-1) \\ \mathbf{A_c} &= e^{\mathbf{A}\cdot T_s}, \quad \mathbf{C} = 1 \\ \mathbf{B_{cu}} &= \int_0^{T_s} e^{\mathbf{A}\cdot t} dt \cdot \mathbf{B_u} \\ \mathbf{B_{cd}} &= \int_0^{T_s} e^{\mathbf{A}\cdot t} dt \cdot \mathbf{B_d} \end{aligned}$$

and $k = int\,(t/T_s)$, t is the running time.

To obtain the predictive output, two assumptions were made: (1) The measurable disturbance remains constant in the prediction horizon, that is $^\circ\Delta d(k+i) = 0, i = 1, 2P-1$; (2) Outside the control horizon, the control variable remains unchanged, that is, $\Delta u(k+i) = 0, i = M, M+1, P-1$, where P is the prediction horizon, and M is the control horizon.

The predictive output in the future is:

$$\mathbf{Y}(k+1|k) = \mathbf{S_x}\Delta x(k) + \mathbf{I}y(k) + \mathbf{S_u}\Delta U(k) + \mathbf{S_d}\Delta d(k) \tag{15}$$

where

$$\mathbf{I} = [1 \cdots 1]_{1\times P}^T$$

$$\mathbf{S}_x = \begin{bmatrix} CA \\ \vdots \\ \sum_{i=1}^{P} CA^i \end{bmatrix}_{P\times 1}$$

$$\mathbf{S}_d = \begin{bmatrix} CB \\ \vdots \\ \sum_{i=1}^{P} CA^{i-1}B \end{bmatrix}_{p\times 1}$$

$$\mathbf{S}_u = \begin{bmatrix} CB & 0 & 0 \\ \vdots & \vdots & \vdots \\ \sum_{i=1}^{P} CA^{i-1}B & \cdots & \sum_{i=1}^{P+M-1} CA^{i-1}B \end{bmatrix}_{P\times M}$$

The sequence of predictive output $\mathbf{Y}(k+1|k)$ is as follows:

$$\mathbf{Y}(k+1|k) = \begin{bmatrix} y(k+1|k) \\ y(k+2|k) \\ \vdots \\ y(k+P|k) \end{bmatrix}_{P\times 1} \tag{16}$$

where each vector of $\mathbf{Y}(k)$ is an array of system output y.

The optimal sequence of control input $\Delta\mathbf{U}(k)$ is as follow:

$$\Delta\mathbf{U}(k|k) = \begin{bmatrix} \Delta u(k|k) \\ \Delta u(k+1|k) \\ \vdots \\ \Delta u(k+M-1|k) \end{bmatrix}_{M\times 1} \tag{17}$$

The reference yaw rate is defined as follow:

$$\mathbf{R}(k+1|k) = \begin{bmatrix} \gamma_{ref}(k+1|k) \\ \gamma_{ref}(k+2|k) \\ \vdots \\ \gamma_{ref}(k+P|k) \end{bmatrix}_{P\times 1} \quad (18)$$

where the reference yaw rate is calculated using (9).

For S-LTVMPC, the reference yaw rate is constant over the prediction horizon.

B. LTVMPC CONTROLLER DESIGN

S-LTVMPC shows good control performance when the tire force is far from the saturation region, that is, the stable region in Fig. 4. However, when vehicle drives near the handing limits, the control effect of S-LTVMPC will worsen, because it assumes a physically unfeasible lateral force, as shown in the blue line in Fig. 7(a). The tire model remains constant in the future prediction process once it is linearized at the current tire slip angle α_j^*. At the predictive time $k+1$, S-LTVMPC assumes that the lateral force is $F_{y,j}^{k+1}$ at the tire slip angle α_j^{k+1}. For the convenience of description, we assume that the tire slip angle changes in the positive direction. However, S-LTVMPC assumes that the lateral force is $F_{y,j}^{k+2,e}$ at the tire slip angle α_j^{k+2} at the predictive time $k+2$, which significantly deviated from the actual value. Especially, when the tire force reaches its limit, S-LTVMPC cannot represent the inversely changing relationship between the tire slip angle and lateral force over the prediction horizon. S-LTVMPC will assume a greater lateral force $F_{y,j}^{k+P,e}$ at α_j^{k+P}, which far exceeds the maximum tire force. At the predictive time $k+P$, to track the reference yaw rate, S-LTVMPC will output a larger front steering angle, and the tire slip angle will also become larger. This phenomenon will lead to a sharp drop in the lateral tire force.

To avoid this situation, we apply the successive linearization of the nonlinear tire model over the prediction horizon (Fig. 7(b)) as follows:

$$\begin{aligned} F_{y,j}^{k+1|k} &= F_{y,j}^{0,k|k} + C_j^{k|k}\cdot\alpha_j^{k|k} \\ F_{y,j}^{k+2|k} &= F_{y,j}^{0,k+1|k} + C_j^{k+1|k}\cdot\alpha_j^{k+1|k} \\ &\vdots \\ F_{y,j}^{k+P|k} &= F_{y,j}^{0,k+P-1|k} + C_j^{k+P-1|k}\cdot\alpha_j^{k+P-1|k} \end{aligned} \quad (19)$$

where

$$\begin{aligned} F_{y,j}^{k|k} &= F_{y,j}^*, F_{y,j}^{0,k|k} = F_{y,j}^{0,*}, \alpha_j^{k|k} = \alpha^* \\ C_j^{k+i|k} &= C_j^{k+i-1|k} + \rho^{k+i|k}\cdot\Delta C_j^k \\ F_{y,j}^{0,k+i|k} &= F_{y,j}^{0,k+i-1|k} + \xi^{k+i|k}\cdot\Delta F_{y,j}^{0,k} \\ \Delta C_j^k &= C_j^k - C_j^{k-1} \\ \Delta F_{y,j}^{0,k} &= F_{y,j}^{0,k} - F_{y,j}^{0,k-1} \quad i = 1,2\cdots P \end{aligned}$$

where $\rho^{k+i|k}$ and $\xi^{k+i|k}$ are regulatory factors that regulate the changes in $C_j^{k+i|k}$ and $F_{y,j}^{0,k+i|k}$ during the prediction process.

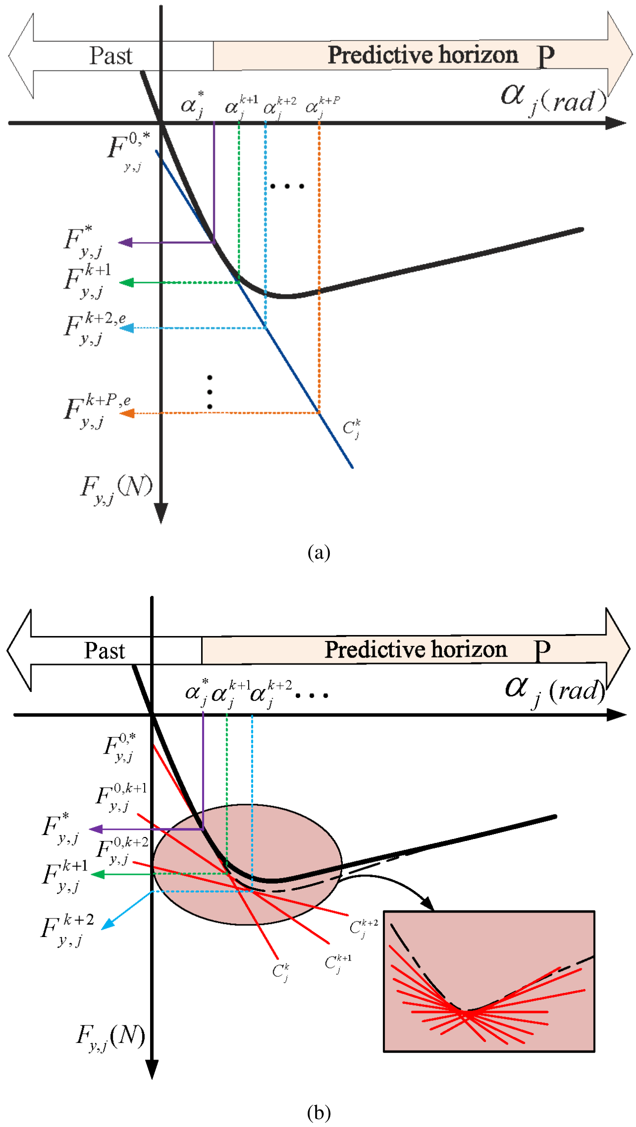

FIGURE 7. Lateral tire force over the prediction horizon. (a) Linearization of S-LTVMPC. (b) Linearization of LTVMPC.

The prediction model for LTVMPC in the prediction horizon can be written as the follows:

$$\dot{\gamma} = \frac{l_f{}^2 C_f^{k+i|k} + l_r{}^2 C_r^{k+i|k}}{V_x I_z}\cdot\gamma + \frac{l_f C_f^{k+i|k} - l_r C_r^{k+i|k}}{I_z}\cdot\beta - \frac{l_f C_f^{k+i|k}}{I_z}\cdot\delta_f + \frac{l_f}{I_z}F_{y,f}^{0,k+i|k} - \frac{l_r}{I_z}F_{y,r}^{0,k+i|k} \quad (20)$$

The prediction model can be written in state-space form as follows:

$$\begin{aligned} \dot{x}(t) &= \mathbf{A_t}x(t) + \mathbf{B_{t,u}}u(t) + \mathbf{B_{t,d}}d(t) \\ y(k) &= x(t) \end{aligned} \quad (21)$$

where

$$\begin{aligned} x &= \gamma, \quad u = \delta_f \\ d &= \left[\beta, F_{y,f,j}^{0,k+i|k}, F_{y,r,j}^{0,k+i|k}\right] \end{aligned}$$

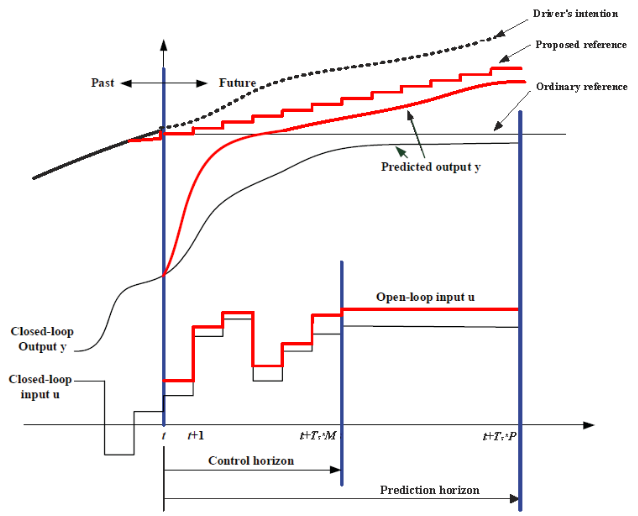

FIGURE 8. Schematic diagram of reference yaw rate considering the driver's intention.

$$\mathbf{A_t} = \frac{{l_f}^2 C_f^{k+i|k} + {l_r}^2 C_r^{k+i|k}}{V_x I_z}$$

$$\mathbf{B_{t,u}} = -\frac{l_f C_f^{k+i|k}}{I_z}$$

$$\mathbf{B_{t,d}} = \left[\frac{l_f C_f^{k+i|k} - l_r C_r^{k+i|k}}{I_z}, \frac{l_f}{I_z}, -\frac{l_r}{I_z}\right]$$

Given that the driver's intention is constantly changing during the prediction process, the reference yaw rate is designed according to the driver's intention on the basis of our previous work [27]. The principle of the designed reference yaw rate is shown in Fig. 8, and it is calculated as follows:

$$\begin{aligned}
\gamma_{ref}(k+1) &= \gamma_{ref}(k) \\
&\quad + \lambda(\gamma_{ref}(k) - \gamma_{ref}(k-1)) \\
\gamma_{ref}(k+2) &= \gamma_{ref}(k+1) \\
&\quad + \lambda(\gamma_{ref}(k) - \gamma_{ref}(k-1)) \\
&\vdots \\
\gamma_{ref}(k+P) &= \gamma_{ref}(k+P-1) \\
&\quad + \lambda(\gamma_{ref}(k) - \gamma_{ref}(k-1))
\end{aligned} \tag{22}$$

where $\gamma_{ref}(k)$ is the reference yaw rate calculated using (9), $\gamma_{ref}(k-1)$ is the reference yaw rate value at time $k-1$, and λ is an adjustable weight factor, which affects the trend of γ_{ref} in the prediction horizon and is obtained through simulation experiments. The acquisition of the sequence of predictive output, control input and reference yaw rate can refer to the derivation process of S-LTVMPC.

C. NMPC CONTROLLER DESIGN

In this section, Pacejka tire model is used to design the NMPC controller, and the prediction model for the nonlinear system is expressed as follows:

$$\dot{\gamma} = \frac{l_f F_{y,f} - l_r F_{y,r}}{I_z} \tag{23}$$

where

$$\begin{aligned}
F_{y,f} &= f_{y,f}(\alpha_f, \mu, F_{z,f}) \\
F_{y,r} &= f_{y,r}(\alpha_r, \mu, F_{z,r})
\end{aligned}$$

The nonlinear system prediction model can be rewritten as follows:

$$\begin{aligned}
\dot{x} &= f(x(t), u(t)) \\
y &= x(t)
\end{aligned} \tag{24}$$

The incremental discrete-time model is consequently given as follows:

$$\begin{aligned}
x(k+1) &= f(x(k), g(\Delta u(k))) \\
y(k) &= x(k) \\
g(\Delta u(k)) &= u(k) - u(k-1)
\end{aligned} \tag{25}$$

The prediction model can be expressed as follows:

$$\begin{aligned}
x(k+1|k) &= f(x(k), g(\Delta u(k))) \\
x(k+2|k) &= f(x(k+1), g(\Delta u(k+1))) \\
&= f(f(x(k), g(\Delta u(k))), g(\Delta u(k+1))) \\
&\vdots \\
x(k+P|k) &= f(x(k+P), g(\Delta u(k+P))) \\
&= f(\cdots f(x(k), g(\Delta u(k)), g(\Delta u(k+M-1)))
\end{aligned} \tag{26}$$

Then, the prediction sequence of output and control input can be obtained. The design of the reference yaw rate is the same as LTVMPC.

D. DESIGN OF COST FUNCTION

The cost function that consists of a weighted combination of yaw rate error and control inputs is defined as follow:

$$\begin{aligned}
J_{mpc} &= \left\|\mathbf{\Gamma_y}(\mathbf{Y}(k+1) - \mathbf{R}(k+1))\right\|^2 + \|\mathbf{\Gamma_u}\Delta\mathbf{U}(k)\|^2 \\
&= \sum_{i=1}^{P}\left[\left(\gamma\ (k+i|k) - \gamma_{ref}\ (k+i)\right)^2 \tau_y\right] \\
&\quad + \sum_{i=1}^{M-1}\left[\left(\Delta\delta_f(k+i-1)^2\right)\tau_u\right]
\end{aligned} \tag{27}$$

where $\mathbf{\Gamma_y} = diag(\tau_y)$ and $\mathbf{\Gamma_u} = diag(\tau_u)$ are weight factors in adjusting tracking performance.

The optimal control problem is described as follow:

$$\begin{aligned}
&\min_{\Delta U(k)}\ J(\mathbf{Y}(k{+}1), \Delta\mathbf{U}(k)) \\
&s.t.\ -u_{\max} \le u\,(k+1+i|k) \le u_{\max} \\
&\qquad -\Delta u_{\max} \le \Delta u\,(k+i|k) \le \Delta u_{\max} \\
&\qquad i = 0, 1, 2\ldots, M-1.
\end{aligned} \tag{28}$$

For S-LTVPC and LTVMPC controllers, the constrained optimization problem is a quadratic programming problem. In this work, it is solved by the trust-region-reflective algorithm. The quadratic programming problem is defined as follows:

$$\min_{\mathbf{x}} \mathbf{x}^{\mathbf{T}}\mathbf{H}\mathbf{x} - \mathbf{g}^{\mathbf{T}}\mathbf{x} \tag{29}$$

$$\mathbf{E}\mathbf{x} < \mathbf{b} \tag{30}$$

where $\mathbf{x} = \Delta\mathbf{U}(k)$, $\mathbf{H}$ is a symmetrical matrix, $\mathbf{g}$ is the gradient vector, and $\mathbf{E}$ and $\mathbf{b}$ are the constraint matrices.

$$\begin{aligned} \mathbf{H} &= 2(\mathbf{S}_{\mathbf{u}}^{\mathbf{T}}\Gamma_{\mathbf{y}}^{\mathbf{T}}\Gamma_{\mathbf{y}}\mathbf{S}_{\mathbf{u}} + \Gamma_{\mathbf{u}}\Gamma_{\mathbf{u}}) \\ \mathbf{g} &= -2\mathbf{S}_{\mathbf{u}}^{\mathbf{T}}\Gamma_{\mathbf{y}}^{\mathbf{T}}\Gamma_{\mathbf{y}}\mathbf{e} \\ \mathbf{e} &= \mathbf{R}(k+1) - \mathbf{S}_{\mathbf{x}}\Delta x(k) - \mathbf{I}y(k) - \mathbf{S}_{\mathbf{d}}\Delta d(k) \\ \mathbf{E} &= [\mathbf{I}^{\mathbf{T}}, -\mathbf{I}^{\mathbf{T}}, \mathbf{L}^{\mathbf{T}}, -\mathbf{L}^{\mathbf{T}}]_{4M\times 1}^{T} \\ \mathbf{b} &= \begin{bmatrix} \Delta\mathbf{U}(k)_{\max} \\ -\Delta\mathbf{U}(k)_{\min} \\ \mathbf{U}_{\max}(k) - u(k-1) \times ones(M,1) \\ u(k-1) \times ones(M,1) - \mathbf{U}_{\min}(k) \end{bmatrix}_{4M\times 1} \end{aligned}$$

For NMPC controller, the nonlinear optimization problem is solved by the sequence quadratic program algorithm.

V. SIMULATION COMPARISON AND ANALYSIS

The simulation experiments are performed based on the cosimulation environment of MATLAB and CarSim on personal computers. B-class hatchback vehicle is selected as the simulation vehicle. Table 1 displays the main parameters of CarSim vehicle.

TABLE 1. Main parameters of CarSim vehicle.

Parameters	Symbol	Value
Distance from COG to front axle	l_f	1.04 m
Distance from COG to rear axle	l_r	1.56 m
Vehicle mass	m	1240 kg
Yaw moment of inertia	I_z	2031.4 kg·m^2
Cornering stiffness of front tire	C_f	−52618 N/rad
Cornering stiffness of rear tire	C_r	−110185 N/rad

The main parameters of the controllers are as follows: where the subscripts *Sine* and *DLC* of the weight coefficients τ_y refer to the weight coefficients under sine and double lane change (DLC) operating conditions, respectively.

A short time step can provide an accurate vehicle dynamics model [25]. And for the stability control of extreme conditions, T_s should be as small as possible. The prediction horizon is the predictive length of the model, and a smaller P is helpful to increase the calculation speed. However, the control effect will be worse. Conversely, the control effect will be better, and the computational burden becomes heavier. M is the dimension of the control variable. The larger it is, the better the control effect is. However, the computational burden will increase and the real-time performance will deteriorate. The values in Table 2 were selected in conjunction with the literature [7], [12], [15] and our experience.

TABLE 2. Main parameters of MPC controllers.

	NMPC	S-LTVMPC	LTVMPC
T_s	0.01	0.01	0.01
P	15	15	15
M	3	3	3
$\delta_{f\ \max}$	15 deg	15 deg	15 deg
$\Delta\delta_{f\ \max}$	0.17	0.12	0.12
$\tau_{y,Sine}$	100	100	100
$\tau_{u,Sine}$	100	450	450
$\tau_{y,DLC}$	100	100	100
$\tau_{u,DLC}$	2800	2000	3000

The simulation times of the proposed three MPC controllers are as follows:

Section V-A and V-B present the simulation results of sine maneuver and DLC maneuver tests, respectively, in which the control performances of S-LTVMPC, LTVMPC and NMPC are compared. In these figures, the olive solid line represents the reference value, the cyan dot dash line is the result of the vehicle with the AFS turned off, whereas the red solid, blue dash and black short dash lines denote the results controlled by NMPC, S-LTVMPC and LTVMPC, respectively.

A. SINE MANEUVER TEST

In this simulation, sinusoidal steering maneuver on snow road ($\mu = 0.3$) is operated, and the vehicle speed is 70 km/h.

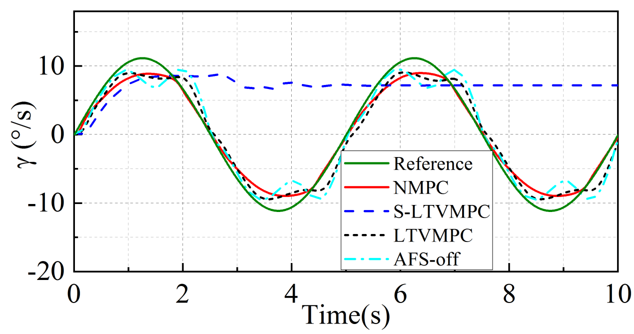

FIGURE 9. Yaw rate.

As shown in Fig. 9, the NMPC can track the reference yaw rate well, and the LTVMPC is close to the tracking effect of NMPC. The maximum tracking deviations of NMPC, LTVMPC, S-LTVMPC and AFS-off are 2.396, 2.621,18.526 and 3.887 respectively. The S-LTVMPC has lost its ability to track the reference yaw rate from $t = 2$ s, because that the S-LTVMPC controller outputs a wrong front steering angle when the actual tire force of the experimental vehicle enters the unstable region, as represented by the blue dash line that shown in Fig. 12. The yaw rate response of AFS-off vehicle has a significant drop near each peak, which indicates that the actual tire force of the experimental vehicle has entered a unstable region, and the lateral tire force is fall, which is insufficient to support high yaw rate. The peak tire force of AFS-off vehicle in Figure 13 can prove this.

Note: The phenomenon that the AFS-off vehicle looks more stable than the S-LTVMPC controlled vehicle. The reasons are: (1) For the AFS-off vehicle, the steering angle is only the drivers open-loop input, which is constant regardless of vehicles state. It wont be adjusted badly like the S-LTVMPC when the tire force enters the unstable region. The vehicle will return to the stable region when the reference yaw rate becomes smaller; (2) There is no mandatory stability constraints imposed on the S-LTVMPC, and the vehicles situation exceeds the working capacity of S-LTVMPC.

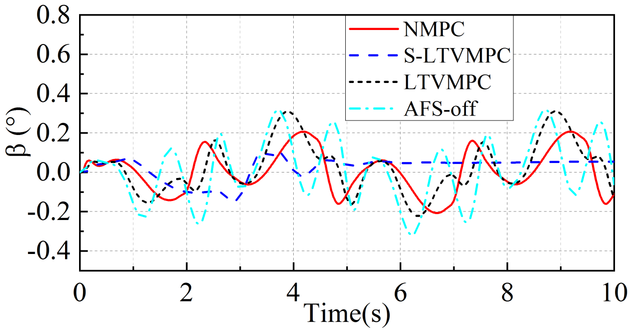

FIGURE 10. Vehicle sideslip angle.

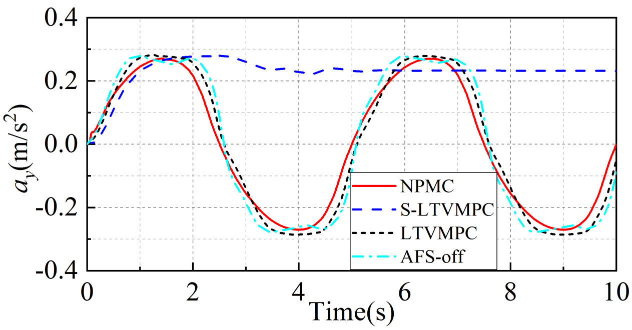

FIGURE 11. Lateral acceleration.

Figs. 10 and 11 are vehicle sideslip angle and lateral acceleration responses, respectively, reflecting the lateral stability of the vehicle. It can be seen from Fig. 10 that both the NMPC and the proposed LTVMPC can suppress the oscillation of the vehicle sideslip angle. The $\beta_{\max}$ and $\beta_{\min}$ of the AFS-off vehicle are 0.318 and −0.318, respectively; that of NMPC are 0.207 and −0.207; that of LTVMPC are 0.310 and −0.223 and that of the S-LTVMPC are 0.102 and −0.146. Although the amplitude of vehicle sideslip angle of the S-LTVMPC is small, it has been kept at 0.05 since about $t = 5.5$ s, indicating that the vehicle has experienced a significant side slip. Fig. 11 shows that the S-LTVMPC controlled vehicle has been unstable from $t = 2$ s.

Fig. 12 shows that both NMPC and LTVMPC can effectively suppress the front wheel steering angles. However, S-LTVMPC outputs a failure front steering angle from $t = 2.5$ s. The reason for this result is that the S-LTVMPC uses the linear tire model to move optimization over the prediction horizon when the actual tire force of the experimental vehicle is in the nonsteady region. A detailed explanation can be found in Section IV-B. A slight drop is present near

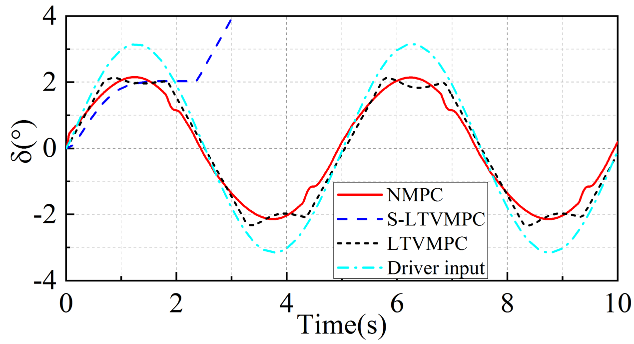

FIGURE 12. Optimized front steering angle.

the peak of the optimized front steering angle of LTVMPC. This result is due to the fact that when the tire force is in the unstable region, the designed LTVMPC will reduce the front steering angle to obtain large lateral force to track the reference yaw rate.

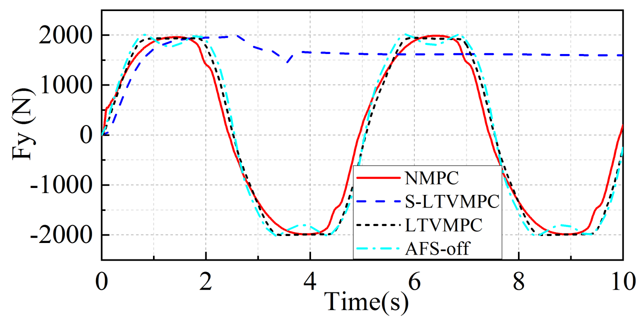

FIGURE 13. Lateral force at front axle.

Fig. 13 shows that the tire force of AFS-off vehicle decreases significantly at the peak, while the tire forces of NMPC and LTVMPC do not fall. The tire of the vehicle controlled by S-LTVMPC is close to saturation since $t = 2$ s, and has remained at around 1600 N since $t = 4$ s. Therefore, LTVMPC can prevent the front axle of the vehicle from sliding and is close to the control effect of NMPC.

B. DLC MANEUVER TEST

To verify the effectiveness of the proposed LTVMPC controller further, the DLC manipulation test was carried out on a road with a tire-road friction coefficient of 0.5. The longitudinal speed of the vehicle was 100 km/h.

In addition, there is a target path in the DLC maneuver test. The steering angle for calculating the reference yaw rate is derived from the built-in driver model of CarSim with the tire-road friction coefficient of 0.85. At the same time, we use this steering angle as the input to the AFF-off vehicle. Therefore, in this test, the driver's input of the AFF-off vehicle can still be regarded as an open-loop input.

Fig. 14 shows that the S-LTVMPC controlled vehicle loses its tracking ability after $t = 4$ s. However, NMPC and LTVMPC controlled vehicles can effectively track the reference yaw rate. The maximum tracking deviations of NMPC,

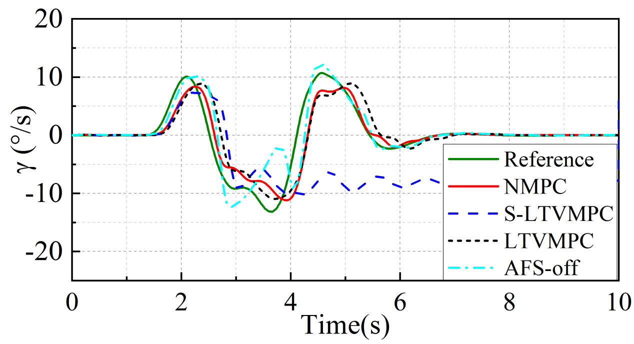

FIGURE 14. Yaw rate.

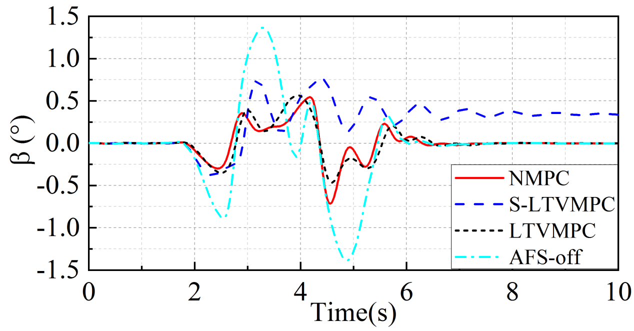

FIGURE 15. Vehicle sideslip angle.

LTVMPC, S-LTVMPC and AFS-off are 9.704, 9.512, 18.222 and 10.554, respectively. It should be noted that the large tracking deviation of NMPC and LTVMPC is mainly due to the delay of the system.

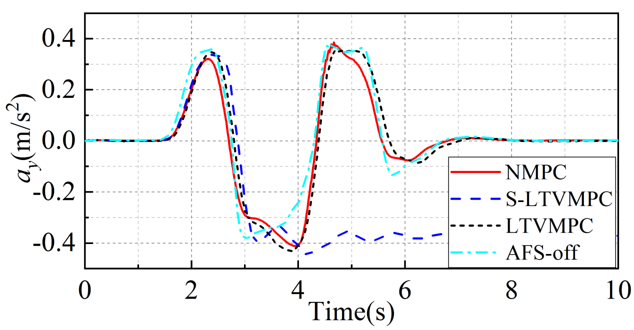

FIGURE 16. Lateral acceleration.

It can be seen from Fig. 15 that vehicle sideslip angle of AFS-off vehicle reached 1.37 and -1.39 at 3.3 and 4.85 seconds, respectively. The control effect of NMPC and LTVMPC are remarkable. However, for S-LTVMPC, the delay of vehicle sideslip angle response is more serious, and it remains unchanged at around 0.35 after $t = 7.5$ s. Fig. 16 shows the simulation results of the lateral acceleration response. It can be found that the control effect of LTV-MPC has a significant improvement compared to the S-LTV-MPC, and it can achieve the control effect of the NMPC.

Fig. 17 and 18 provide the simulation of the front steering angles and lateral force of front axle, respectively. Similar results found in previous test can also be observed in this maneuver.

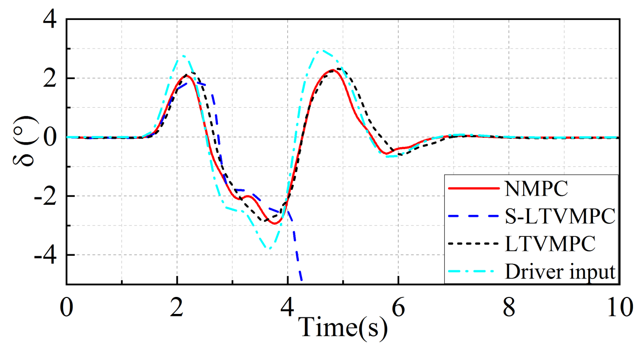

FIGURE 17. Optimized front steering angle.

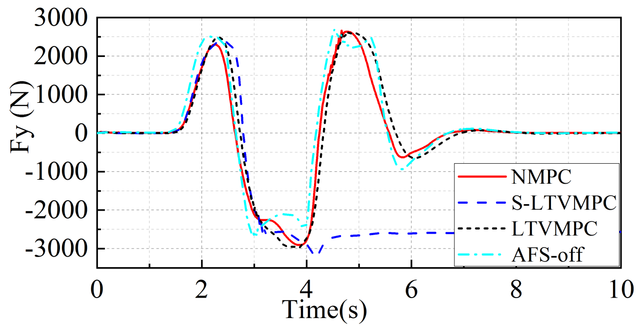

FIGURE 18. Lateral force at front axle.

TABLE 3. Controllers simulation time.

	NMPC	S-LTVMPC	LTVMPC
Time	65.8 s	28.1 s	37.9 s

On the basis of the simulation results, we can conclude that the proposed LTVMPC can not only effectively prevent the vehicle from sliding but also improve the vehicle response compared with S-LTVMPC at the handling limits. In addition, on the basis of the simulation time of the three controllers shown in Table 3, NMPC takes the longest time, followed by LTVMPC and S-LTVMPC. Therefore, the designed LTVMPC can reach the control effect of NMPC, reduce the computational burden, and improve the real-time performance.

VI. CONCLUSION

This paper proposes a LTVMPC approach based on the changing trend of tire force to improve the handling and stability of AFS vehicles at the limits of vehicle dynamics. The nonlinear control effect is achieved, and the computational burden is reduced by linearizing the nonlinear tire model and considering the change trend in the prediction horizon successively. In the future, we will adopt this method to design an adaptive steering and braking-integrated control system with time-varying system constraints to improve vehicle handing and stability performance.

REFERENCES

[1] M. Doumiati, O. Sename, L. Dugard, J.-J. Martinez-Molina, P. Gaspar, and Z. Szabo, "Integrated vehicle dynamics control via coordination of active front steering and rear braking," *Eur. J. Control*, vol. 19, no. 2, pp. 121–143, 2013.

[2] S. Yim, S. Kim, and H. Yun, "Coordinated control with electronic stability control and active front steering using the optimum yaw moment distribution under a lateral force constraint on the active front steering," *Proc. Inst. Mech. Eng. D, J. Automobile Eng.*, vol. 230, no. 5, pp. 581–592., 2016.

[3] Y. Ji, H. Guo, and H. Chen, "Integrated control of active front steering and direct yaw moment based on model predictive control," in *Proc. Control Decis. Conf.*, May/Jun. 2014, pp. 2044–2049.

[4] S. Di Cairano, H. E. Tseng, D. Bernardini, and A. Bemporad, "Vehicle yaw stability control by coordinated active front steering and differential braking in the tire sideslip angles domain," *IEEE Trans. Control Syst. Technol.*, vol. 21, no. 4, pp. 1236–1248, Jul. 2013.

[5] Y. Ji, H. Guo, and H. Chen, "Integrated control of active front steering and direct yaw moment for enhancing lateral vehicle stability," in *Proc. Int. Conf. Mechatron. Control*, Jul. 2015, pp. 1078–1083.

[6] S. Yim, "Coordinated control of ESC and AFS with adaptive algorithms," *Int. J. Automot. Technol.*, vol. 18, no. 2, pp. 271–277, 2017.

[7] M. Jalali, S. Khosravani, A. Khajepour, S.-K. Chen, and B. Litkouhi, "Model predictive control of vehicle stability using coordinated active steering and differential brakes," *Mechatronics*, vol. 48, pp. 30–41, Dec. 2017.

[8] S. Mammar and D. Koenig, "Vehicle handling improvement by active steering," *Vehicle Syst. Dyn.*, vol. 38, no. 3, pp. 211–242, 2002.

[9] Y. H. Xu and M. Ahmadian, "Study on the performance of active front steering system," *Int. J. Automot. Technol.*, vol. 14, no. 4, pp. 595–603, 2013.

[10] D. V. T. Truong and W. Tomaske, "Active front steering system using adaptive sliding mode control," in *Proc. Control Decis. Conf.*, May 2013, pp. 253–258.

[11] A. Elhefnawy, A. H. Sharaf, H. Ragheb, and S. Hegazy, "Integrated vehicle chassis control based on direct yaw moment and active front steering," in *Proc. Int. Conf. Appl. Mech. Mech. Eng.*, 2016, pp. 1–19.

[12] P. Falcone, F. Borrelli, J. Asgari, H. E. Tseng, and D. Hrovat, "Predictive active steering control for autonomous vehicle systems," *IEEE Trans. Control Syst. Technol.*, vol. 15, no. 3, pp. 566–580, May 2007.

[13] H. Chen, *Model Predictive Control*. Beijing, China: Science Press, 2013.

[14] D. Hrovat, S. Di Cairano, H. E. Tseng, and I. V. Kolmanovsky, "The development of model predictive control in automotive industry: A survey," in *Proc. IEEE Int. Conf. Control Appl.*, Oct. 2013, pp. 295–302.

[15] C. E. Beal and J. C. Gerdes, "Model predictive control for vehicle stabilization at the limits of handling," *IEEE Trans. Control Syst. Technol.*, vol. 21, no. 4, pp. 1258–1269, Jul. 2012.

[16] F. Borrelli, P. Falcone, T. Keviczky, J. Asgari, and D. Hrovat, "MPC-based approach to active steering for autonomous vehicle systems," *Int. J. Vehicle Auton. Syst.*, vol. 3, nos. 2–4, pp. 265–291, 2005.

[17] P. Falcone, H. E. Tseng, F. Borrelli, J. Asgari, and D. Hrovat, "MPC-based yaw and lateral stabilisation via active front steering and braking," *Vehicle Syst. Dyn.*, vol. 46, pp. 611–628, Sep. 2008.

[18] W. H. Chen, D. J. Ballance, and J. O'Reilly, "Model predictive control of nonlinear systems: Computational burden and stability," *IEE Proc.-Control Theory Appl.*, vol. 147, no. 4, pp. 387–394, Jul. 2002.

[19] P. Falcone, M. Tufo, F. Borrelli, J. Asgari, and H. E. Tseng, "A linear time varying model predictive control approach to the integrated vehicle dynamics control problem in autonomous systems," in *Proc. IEEE Conf. Decis. Control*, Dec. 2007, pp. 2980–2985.

[20] P. Falcone, F. Borrelli, H. E. Tseng, J. Asgari, and D. Hrovat, "Linear time-varying model predictive control and its application to active steering systems: Stability analysis and experimental validation," *Int. J. Robust Nonlinear Control*, vol. 18, no. 8, pp. 862–875, 2008.

[21] S. Velhal and S. Thomas, "Improved LTVMPC design for steering control of autonomous vehicle," *J. Phys. Conf. Ser.*, vol. 783, p. 012028, Jan. 2017.

[22] M. Choi and S. B. Choi, "MPC for vehicle lateral stability via differential braking and active front steering considering practical aspects," *Proc. Inst. Mech. Eng. D, J. Automobile Eng.*, vol. 230, no. 4, pp. 459–469, 2016.

[23] M. Choi and S. B. Choi, "Model predictive control for vehicle yaw stability with practical concerns," *IEEE Trans. Veh. Technol.*, vol. 63, no. 8, pp. 3539–3548, Oct. 2014.

[24] S. M. Erlien, S. Fujita, and J. C. Gerdes, "Shared steering control using safe envelopes for obstacle avoidance and vehicle stability," *IEEE Trans. Intell. Transp. Syst.*, vol. 17, no. 2, pp. 441–451, Feb. 2016.

[25] J. Funke, M. Brown, S. M. Erlien, and J. C. Gerdes, "Collision avoidance and stabilization for autonomous vehicles in emergency scenarios," *IEEE Trans. Control Syst. Technol.*, vol. 25, no. 4, pp. 1204–1216, Jul. 2016.

[26] M. Brown, J. Funke, S. Erlien, and J. C. Gerdes, "Safe driving envelopes for path tracking in autonomous vehicles," *Control Eng. Pract.*, vol. 61, pp. 307–316, Apr. 2017.

[27] S. Zheng *et al.*, "MPC based driver's intention prediction method for vehicle stability control," in *Proc. Int. Conf. Automat., Mech. Elect. Eng.*, 2017, pp. 209–213.

[28] Y. F. Yu, *Vehicle System Dynamics*. Beijing, China: China Machine Press, 2000.

[29] Z. Yu, *Automotive Theory*. Beijing, China: Machinery Industry Press, 2009.

[30] H. B. Pacejka, *Tire and Vehicle Dynamics*. Amsterdam, The Netherlands: Elsevier, 2006.

[31] J. Chen, L. Li, and J. Song, "A study on vehicle stability control based on LTV-MPC," *Automot. Eng.*, vol. 38, pp. 308–316, Mar. 2016.

[32] B. Ren, H. Chen, H. Zhao, and L. Yuan, "MPC-based yaw stability control in in-wheel-motored EV via active front steering and motor torque distribution," *Mechatronics*, vol. 38, pp. 103–114, Sep. 2016.

SHAOSONG LI received the Ph.D. degree in automotive engineering from Jilin University, Jilin, China, where he focused on vehicle dynamics and control. He is a member of the Society of Automotive Engineers of China.

He is currently a Teacher with the Changchun University of Technology. His current research interests include the application of control systems to vehicle dynamics to improve safety, stability, and the performance of vehicles in conjunction with human drivers.

He was a recipient of the Jilin Province Science and Technology Found for Young Scholars and the Ministry of Education Chun hui Plan.

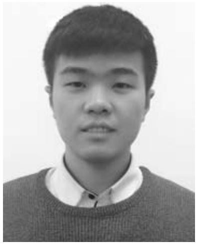

GUODONG WANG received the bachelor's degree in automotive engineering from Huanghe Science and Technology College, Henan, China. He is currently pursuing the master's degree in automotive engineering from the Changchun University of Technology, Jilin, China.

His research interest includes the theory and technology of automotive safety and model predictive control.

BANGCHENG ZHANG received the B.Eng. and M.Eng. degrees from the Changchun University of Technology, Changchun, China, in 1995 and 2004, respectively, and the Ph.D. degree from Jilin University, Changchun, China, in 2011. He was an Academic Visitor with Tsinghua University, Beijing, China, in 2007. He is currently a Professor with the Changchun University of Technology, Changchun. He has published about 20 articles. His research interests include mechatronics measurement technique and fault diagnosis.

His research interest includes the theory and technology of vehicle and model predictive control.

ZHIXIN YU received the Ph.D. degree in automotive engineering from Jilin University, Jilin, China, where he focused on heavy duty vehicle rollover detection and active roll control.

He is currently a Teacher with the Changchun University of Technology. His current research interests include the application of control systems to vehicle dynamics to improve stability and the rollover stability analysis of tank vehicles.

GAOJIAN CUI received the Ph.D. degree in mechanical design and theory from the Changchun University of Science and Technology, Jilin, China. He is currently the Vice President of the Automotive Engineering Research Institute, Changchun University of Technology. His current research interests include model-based vehicle dynamics control and intelligent vehicle path planning and tracking.

He was a recipient of the Key Technology on Major Program of Jilin Province.